COMMUNICATION

Bottom-up synthesis of $Zn_{1.7}GeN_{1.8}O$ nanoparticles for photocatalytic application†

Constanze Schliehe and Cristina Giordano*

Via a simple bottom-up approach, a complex quaternary oxynitride system ($Zn_{1.7}GeN_{1.8}O$) was prepared in the form of small nanoparticles ($d \sim 15$ nm), which were stable and morphologically well-defined. The $Zn_{1.7}GeN_{1.8}O$ nanoparticles exhibited a band gap of 2.4 eV and were active towards photocatalytic degradation of organic dyes.

In recent decades, research into sustainable technologies, in various fields, has risen significantly. In this context, catalytic nanomaterials have attracted considerable attention. Reducing the required reaction energy and accelerating the overall reaction kinetics allow these materials to be utilized in various applications.[1,2] Classical catalytic materials are often designed from noble metals such as platinum, palladium, or gold.[3,4] In the 1970s Levy and Boudart investigated the catalytic activity of some metal carbides with isoelectronic properties similar to that of noble metals (*e.g.* tungsten carbide *vs.* platinum.).[5,6] Metal carbides, as well as their related nitrides, are promising materials with properties such as superior hardness, strength, and corrosion resistance. Furthermore, their electronic character may be influenced by chemical composition changes, which allow for the design of materials with metallic, semiconducting, or isolating properties.[7] In addition, a number of transition metal nitrides or oxynitrides were demonstrated to have photocatalytic behaviors, which was accredited to their favorable band gap energies.[8]

The advantage of metal oxynitrides lies in the possibility of adjusting their band gap (*i.e.* by adjusting the nitrogen loading). While the pure oxides usually have high band gap energy and

the nitrides a low one, oxynitrides often have an intermediate band gap with energies corresponding to the visible light range. This is a consequence of combining nitrogen's (N) 2p orbitals with that of oxygen's (O) 2p orbitals.[9] As with all photosensitive semiconducting materials, light irradiation can lead to an excitation of electron(s) from the valence band into the conducting band. The newly formed exciton migrates to the surface affording the opportunity for oxidation or reduction reactions to occur with the electron or the corresponding hole. These reactions can be, for example, utilized towards hydrogen production (*via* splitting water molecules),[10] the reduction of nitrogen oxides[11] or the degradation of organic molecules.[12]

Depending on the respective required energy, the band gap of the catalytic metal oxynitride material can be adjusted. This offers the possibility of efficiently using solar energy to produce renewable energy sources or of clearing air and water from pollutants.

Typical photocatalytic oxide, nitride, and oxynitride materials are d^0 based compounds (*e.g.* TiO_2,[13] Ta_3N_5,[14] $BaTaO_2N$,[15] *etc.*). Recently, the interest in d^{10} based materials like $(Ga_{1-\chi}Zn_\chi)(N_{1-\chi}O_\chi)$, Ge_3N_4 or $Zn_{(1+\chi)}GeN_2O_\chi$ has increased.[16,17] Due to hybridized s and p orbitals of the metal and the lower conducting levels, the mobility of the electrons is increased, resulting in a higher photocatalytic activity.[18,19] Although the catalytic capability of the transition metal nitrides and oxynitrides is high, the availability of nanocrystals of these materials is still rare due to the high demands on the synthetic procedure.

Classical approaches for the synthesis of nitride-based materials are metathesis,[20] thermal decomposition,[21] or ammonolysis.[22] The use of toxic ingredients, high reaction temperatures, and long reaction times results in poor shape control and the lack of homogeneity of the product particles. For example, $Zn_{(1+\chi)}GeN_2O_\chi$, a semiconducting material with a band gap of 2.5–2.7 eV, is a heterogeneous solid state solution of $ZnGeN_2$ (bg: 3.3 eV) and ZnO (bg: 3.2 eV) and currently there are only a few synthetic procedures described in the literature. Typically, different zinc and germanium oxide powders are

Max Planck Institute for Colloids and Interfaces, Am Mühlenberg 1, 14476 Potsdam, Germany. E-mail: cristina.giordano@mpikg.mpg.de; Fax: +49-(0)-331-567-9502; Tel: +49-(0)-331-567-9509

† Electronic supplementary information (ESI) available: SEM of the particles; absorption spectra; BET plot; TEM and XRD of the particles of the up-scaled synthesis; TEM of particles synthesized in the absence of ammonium chloride; IR-spectra; TGA plot; TEM of particles synthesized at 600 °C; elemental analysis. See DOI: 10.1039/c3nr33561e

nitrided to form the product material.[23] For example, at a temperature of 1123 K the reaction of GeO_2 and ZnO under ammonia flow leads to the formation of the desired product, but in the form of aggregates between 200 and 300 nm.[23] Mesoporous $Zn_{(1+\chi)}GeN_2O_\chi$ can be synthesized by nitridation of Zn_2GeO_4 under ammonia flow where surface areas of 24.4 m^2 g^{-1} were obtained.[24] The ammonolysis of zinc and germanium oxides produced structures with surface areas between 7.5 and 31 m^2 g^{-1}.[25]

Some years ago, our group set up the soft urea pathway, a simple bottom-up approach for the synthesis of metal nitrides and carbides, which avoids the use of toxic reactants, high temperatures, and long reaction times.[7,26,30] In this one pot procedure the molecular metal precursor, ethanol, and urea form a glassy phase, which is then calcined under an inert atmosphere.[27] Urea here resumes the role as a coordination agent as well as provides the source of nitrogen, or carbon, in the final material. The bottom-up approach enables us to control nucleation and growth during the synthesis resulting in the formation of homogeneous, nanocrystalline particles. In the last few years, we have applied and presented this pathway for several binary metal nitrides and carbides; some examples include Fe_3C, WC, Fe_3N, Ta_3N_5 or Mo_2N.[28–30] The next step now is to transfer this established procedure to more complex systems like ternary or quaternary carbides and nitrides.

Herein, we present the simple and sustainable bottom-up synthesis of stable quaternary $Zn_{1.7}GeN_{1.8}O$ nanoparticles *via* the soft urea pathway. To the best of our knowledge, this is the first reported method towards a quaternary nitride material *via* a bottom-up approach. Crystalline and homogeneous products were obtained from water soluble metal precursors, in the presence of urea and ammonium chloride, and heated to 800 °C under an inert atmosphere. We studied the influence of ammonium chloride on the crystallization process and determined its ability of tuning the nucleation and growth behavior. We applied the as-synthesized $Zn_{1.7}GeN_{1.8}O$ nanopowder to a photocatalytic material and observed the degradation of rhodamine B. The catalytic efficiency of the as-prepared $Zn_{1.7}GeN_{1.8}O$ particles illustrates comparable results to other currently described catalytic nanoparticle systems in the literature, providing an alternative, sustainable, approach towards the synthesis of such materials.

With the soft urea glass route, and a simultaneous use of two different molecular metal precursors, we were able to access ternary and/or quaternary compounds like $Zn_{1.7}GeN_{1.8}O$. The addition of ammonium chloride to the initial mixture (for details see Experimental section) improved the quality of the product and led to the formation of single phase and monodisperse $Zn_{1.7}GeN_{1.8}O$ nanostructures. The transmission electron microscope (TEM) images in Fig. 1A and B display the as-synthesized homogeneous $Zn_{1.7}GeN_{1.8}O$ particles prepared in the presence of ammonium chloride. The particles are rather monodisperse in shape and size. The histogram depicted in the inset of Fig. 1A illustrates the statistic size distribution of the particles with an average diameter of 15 nm, close to the calculated size (~10 nm) by the X-ray diffraction (XRD) *via* the full width at half maximum (FWHM). The homogeneity of
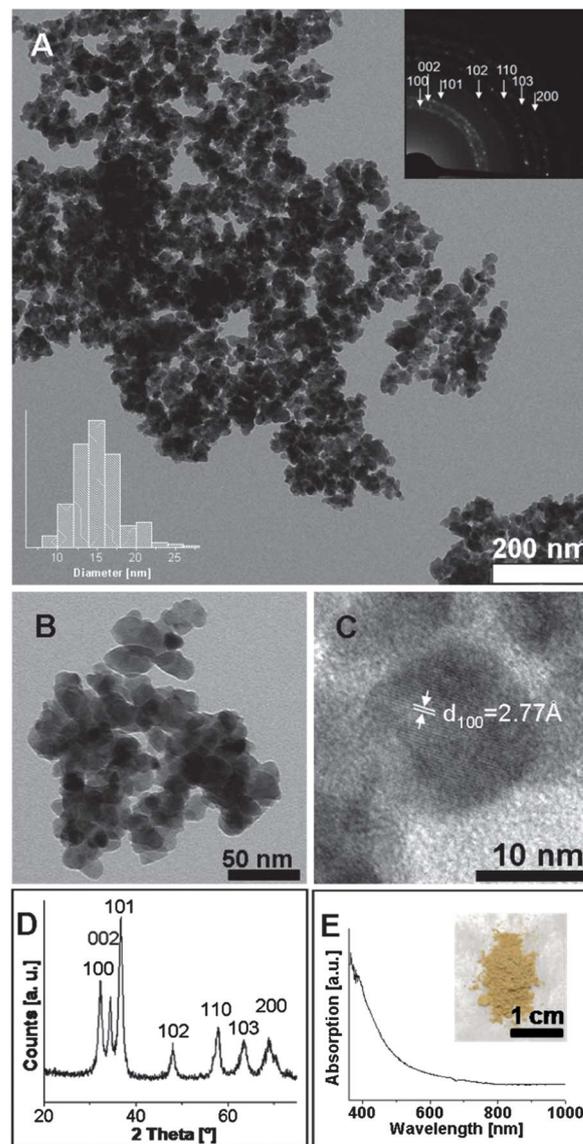

Fig. 1 (A and B) TEM images of $Zn_{1.7}GeN_{1.8}O$ particles at different resolutions. The insets of A show a SAED with the typical pattern of $Zn_{1.7}GeN_{1.8}O$ and a histogram of the size distribution. (C) High resolution TEM image of a particle highlighting lattice fringes in a grain oriented along the (100) plane. (D) XRD of $Zn_{1.7}GeN_{1.8}O$ (ICDD 00-024-1443). (E) Absorption spectra and an image of the sample in the inset.

the overall sample was supported by scanning electron microscope (SEM) imaging (see Fig. S1†). Due to the crystallinity of the $Zn_{1.7}GeN_{1.8}O$ particles, lattice fringes were observed in the HR-TEM image (Fig. 1C). The distance of the lattice fringes were measured to be 2.77 Å, which corresponds to the lattice distance for $Zn_{1.7}GeN_{1.8}O$ crystal particles.[31] The XRD spectrum is illustrated in Fig. 1D and the selected area electron diffraction (SAED) pattern is presented in the inset of Fig. 1A. Combined, these solid state analytical techniques support the crystallinity of the sample and identify the material as $Zn_{1.7}GeN_{1.8}O$ (ICDD 00-024-1443). From the absorption spectra (Fig. 1E) of the yellowish product (inset), an energy band gap of 2.4 eV was calculated (see Fig. S2†). Furthermore, we characterized the

$Zn_{1.7}GeN_{1.8}O$ powder by Brunauer–Emmett–Teller (BET) surface area measurements and obtained a value of 51 m^2 g^{-1} (see Fig. S3†). This is up to five times larger than the surface areas that were previously reported for the $Zn_{(1+\chi)}GeN_2O_\chi$ particles, prepared under harsh reaction conditions (*i.e.* ammonia flow, high temperatures and long reaction times). The present route has several advantages: it is simple, cheap, environmentally friendly and sustainable. Furthermore, since scalability is of utmost importance for industrial purposes, we used the tenfold amount of the ingredients and found out that the quality and the characteristics of the particles did not change (see Fig. S4†). It should be however pointed out that the composition and purity of the product are very sensitive to the composition of the initial reaction mixture. Small variations in the precursor concentrations lead to the formation of mixtures, where germanium, germanium nitride, zinc germanium oxide or zinc cyanide were obtained as side products.

In order to understand the role that ammonium chloride plays in controlling the particle structure, various experiments were performed. In particular, the temperature dependent evolution of the reaction mixtures was investigated by infrared spectroscopy, elemental analysis, thermogravimetric measurements, XRD and TEM. For comparison, results of samples prepared without ammonium chloride are also reported *vide infra*.

The starting material in both cases, with and without ammonium chloride, appeared colorless and "glassy". The urea served as a secondary coordination agent for the metal ions in the starting complex *via* hydrogen bridges and Coulomb interactions, as previously reported.[7] The IR-spectra of this starting phase share similar wavenumbers to the product (*e.g.* broadening in the N–H vibration band) supporting the inclusion of ammonium chloride into the glassy structure disfavoring an interaction with the metal ions, where a reduced signal intensity of the amide would have been observed (see Fig. S6A and B†). The thermogravimetric analyses of the two systems in the range of 25–1000 °C under nitrogen showed crucial differences in the dependency of the mass loss on the reaction temperature (see Fig. S7†). In the first step up to 300 °C the mass change amounts to 57% and 45% respectively. Presumably, the mass change was dominated by the decomposition of urea alongside the formation of an ammonium rich atmosphere. In the presence of ammonium chloride this effect is almost 30% higher. The ability of ammonium chloride to increase the local ammonia amount during the reaction has been described before.[32,33] In the second step, a further mass loss of 19% and 18%, respectively, was observed. In the case of the reaction without ammonium chloride the mass change was continuous, while in the presence of ammonium chloride it was sigmoidal, due to its decomposition temperature of 338 °C. Finally, 24% and 37% of the original masses, respectively, remained. The variance in the final mass may have been caused by the different organic content in the starting material's composition.

The presence of ammonium chloride, and thus an increased content of ammonia in the atmosphere, resulted in a change in the crystallization behavior at lower temperatures. For the analysis of the crystallization behavior the reaction was quenched at different temperatures, the XRDs are plotted in
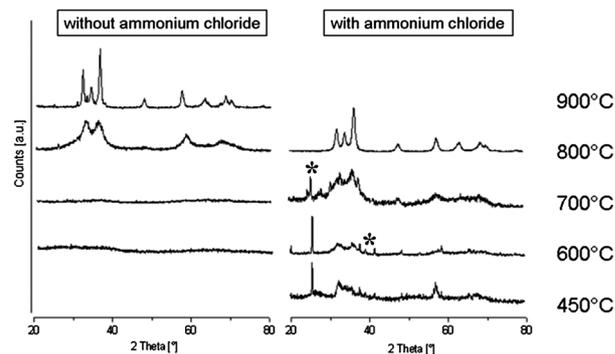

Fig. 2 X-ray diffractograms of the reactions quenched at different temperatures. Left: without ammonium chloride; right: with ammonium chloride. The reflexes were identified as $Zn_{1.7}GeN_{1.8}O$ (ICDD 00-024-1443) and marked peaks as GeO_2 (ICDD 00-043-1016).

Fig. 2. In the absence of ammonium chloride no crystalline features can be detected below the reaction temperature of 800 °C whereas at 900 °C the final composition and crystal size of $Zn_{1.7}GeN_{1.8}O$ (ICDD 00-024-1443) were achieved. In contrast, in the presence of ammonium chloride, an alternative crystallization behavior was observed; crystalline features were visible in the XRD spectra by 450 °C. The additional lattice reflections were suggestive towards GeO_2 particles (ICDD 00-043-1016). The final reaction product was achieved at 800 °C and no residual GeO_2 was detectable. The extreme broadening of the diffractogram peaks, as related to the particles synthesized at lower temperatures, supports the presence of small nuclei with a diameter of ~3 nm (determined *via* the FWHM). TEM analysis of the sample, prepared with ammonium chloride at 600 °C, illustrates the effect that the additive has towards the formation of homogeneous nanoparticles. For the comparison of the particles synthesized with and without ammonium chloride at 600 °C (see Fig. S8†).

The successful nanoparticle production in the presence of ammonium chloride at lower temperatures adheres to the methodology and design of these materials without additives. This trend was also observed by elemental analysis and infrared spectroscopy. By determining the quotient, with respect to the amount of carbon to nitrogen, we were able to monitor the progress of the reaction. As expected, the values were higher when ammonium chloride was not present in the reaction mixture (due to its nitrogen rich structure). However, once the value approached zero, the carbon free product was achieved. In the presence of ammonium chloride this was accomplished at 800 °C, while in its absence a reaction temperature of around 900 °C was required (see Fig. S9†).

Infrared analysis detected the crucial changes of the organic material during the calcination process. At 300 °C bands of N= C=O and N=C appear, corresponding to the condensation of the urea molecules. Finally, in the presence of ammonium chloride, at 800 °C no features for N–H, C=O, N=C=O or N=C were detectable, confirming that the reaction was complete. In the absence of ammonium chloride the same trend can be observed, but shifted to higher temperatures. Thus, at 800 °C the band intensity significantly decreased.
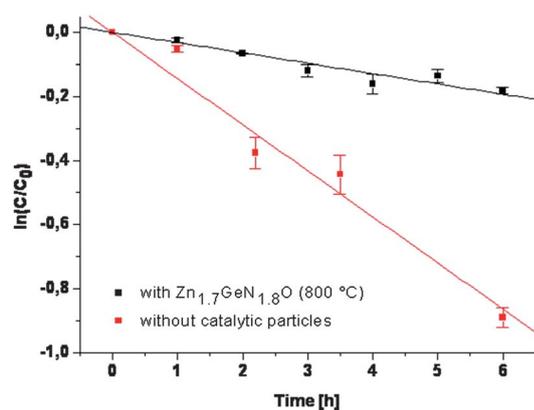
Fig. 3 Photocatalytic degradation of rhodamine B. A plot of log(C/C_0) over the time in hours. The concentration was determined by absorption measurements.

Considering the findings outlined above, the presence of ammonium chloride was accelerating the crystallization process by an additional evolution of ammonia. Thus the nucleation process occurs at low temperatures of around 400 °C (800 °C in the absence), followed by a long growth and ripening process in the temperature range of 400–800 °C (800–900 °C in the absence). This reduction of the nucleation temperature and prolongation of the growth process allow the formation of homogeneous $Zn_{1.7}GeN_{1.8}O$ particles (see Fig. S5†).

According to the band gap energy of 2.4 eV and the relative energies of the valence and the conduction band, $Zn_{1.7}GeN_{1.8}O$ represents a potential catalyst for photocatalytic reactions. To test its photocatalytic properties, $Zn_{1.7}GeN_{1.8}O$ particles were applied for the photocatalytic degradation of rhodamine B, a model system for removing pollution from water.[12] The test of the activity for the photocatalytic degradation of rhodamine B with $Zn_{1.7}GeN_{1.8}O$ nanopowder (NH_4Cl; 800 °C) was done in aqueous solution under Hg-lamp irradiation (for details see Experimental section). After exciton formation and migration, the hole was transferred to rhodamine B resulting in a radical cation followed by complete degradation. The decrease of the rhodamine B concentration overtime was determined *via* absorption spectroscopy, and the reaction constant was calculated, assuming first order reaction kinetics.[12] The plot of the logarithmic relationship between the concentration at any given time (C_t) over the initial concentration (C_0) quotient *versus* time is shown in Fig. 3. We determined the reaction constant of the catalyzed degradation to be 0.14 h^{-1}. This value can compete with those that were determined for reactions catalyzed by structures synthesized *via* ammonolysis of ZnO and Ge_2O.[12] The exposure to water and UV-light for several hours did not affect the stability of the catalytic particles. XRD analysis of the particles after the catalytic reaction showed that the composition did not change (see Fig. S10†).

Conclusions

In summary we have presented the synthesis of a complex quaternary oxynitride system (stable $Zn_{1.7}GeN_{1.8}O$ nanoparticles) *via* a simple bottom-up approach. Through the soft urea route procedure with the addition of ammonium chloride, complete control over particle size (as monodisperse systems) was achieved, still utilizing moderate reaction conditions. The ammonium rich atmosphere, evolving with the sublimation of ammonium chloride, resulted in a reduction of the nucleation temperature and the prolongation of the growth and ripening process. Thus crystalline and monodisperse $Zn_{1.7}GeN_{1.8}O$ nanoparticles, with an average diameter of 15 nm, were achieved. The particles exhibit a band gap energy of 2.4 eV and are thus suitable as catalysts for photocatalytic reactions. Exemplarily, we applied the as-prepared $Zn_{1.7}GeN_{1.8}O$ nanoparticles towards the photocatalytic degradation of rhodamine B and determined a reaction constant of 0.14 h^{-1}.

The presented procedure affords the production of small $Zn_{1.7}GeN_{1.8}O$ nanoparticles in a simple and scalable way, while utilizing sustainable reaction conditions such as moderate temperatures and "green" reactants. These results represent a significant improvement, with respect to the few and already known synthetic procedures presently reported in the literature, providing a simple approach towards quaternary compounds, thus extending their applicability and significance in various fields.

Experimental section

The $Zn_{1.7}GeO_{1.8}N$ particles were synthesized with the variation of the urea glass route. In a typical synthesis, zinc acetate (146 mg; 0.6 mmol), germanium(IV) methoxide (50 µL; 0.3 mmol), urea (100 mg; 16 mmol) and ammonium chloride (35 mg; 0.6 mmol) were dissolved in a mixture of water (500 µL) and ethanol (400 µL) to form a homogeneous solution. After the solution was transferred into a crucible, the solvent was evaporated resulting in a white fused phase. The glassy phase was calcined under nitrogen up to 800 °C. After cooling down to room temperature, a yellow powder was obtained.

For the photocatalytic decomposition of rhodamine B the following procedure was used: an aqueous solution of rhodamine B (50 mL water, 5 ppm rhodamine B) was combined with the catalytic $Zn_{1.7}GeO_{1.8}N$ particles (50 mg). The dispersion was treated with Hg-lamp light for several hours. Every hour an aliquot was taken from the solution, the $Zn_{1.7}GeO_{1.8}N$ particles were separated from the solution by centrifugation and the remaining concentration of rhodamine B was determined by absorption spectroscopy.

Acknowledgements

Notes and references

1 A. Roucoux, J. Schulz and H. Patin, *Chem. Rev.*, 2002, **102**, 3757.
2 D. Astruc, F. Lu and J. R. Aranzes, *Angew. Chem., Int. Ed.*, 2005, **44**, 7852.

3 F. F. Ren, W. Q. Zhou, Y. K. Du, P. Yang, C. Y. Wang and J. K. Xu, *Int. J. Hydrogen Energy*, 2011, **36**, 6414.

4 C. H. Chen, W. J. Liou, H. M. Lin, A. Borodzinski, L. Stobinski and P. Kedzierzawski, *Fuel Cells*, 2010, **2**, 227.

5 R. B. Levy and M. Boudart, *Science*, 1973, **181**, 547.

6 J. Lemaitre, B. Vidick and B. Delmon, *J. Catal.*, 1986, **99**, 415.

7 C. Giordano and M. Antonietti, *Nano Today*, 2011, **6**, 366.

8 Q. H. Zhang and L. Gao, *Langmuir*, 2004, **20**, 9821.

9 T. Takata, G. Hitoki, J. N. Kondo, M. Hara, H. Kobayashi and K. Domen, *Res. Chem. Intermed.*, 2007, **33**, 13.

10 K. Takanabe, T. Uzawa, X. Wang, K. Maeda, M. Katayama, J. Kubota, A. Kudo and K. Domen, *Dalton Trans.*, 2009, 10055.

11 N. Imanaka and T. Masui, *Appl. Catal., A*, 2012, **431**, 1.

12 J. Huang, X. Cui and X. Wang, *Environ. Sci. Technol.*, 2010, **44**, 3500.

13 A. Fujishima, T. N. Rao and D. A. Tryk, *J. Photochem. Photobiol., C*, 2000, **1**, 1.

14 G. Hitoki, A. Ishikawa, T. Takata, J. N. Kondo, M. Hara and K. Domen, *Chem. Lett.*, 2002, 736.

15 D. Yamasita, T. Takata, M. Hara, J. N. Kondo and K. Domen, *Solid State Ionics*, 2004, **172**, 591.

16 K. Maeda, T. Takata, M. Hara, N. Saito, Y. Inoue, H. Kobayashi and K. Doman, *J. Am. Chem. Soc.*, 2005, **127**, 8286.

17 J. Sato, N. Saito, Y. Yamada, K. Maeda, T. Takata, J. N. Kondo, M. Hara, H. Kobayashi, K. Domen and Y. Inoue, *J. Am. Chem. Soc.*, 2005, **127**, 4150.

18 J. Sato, N. Saito, H. Nishiyama and Y. Inoue, *J. Phys. Chem. B*, 2001, **105**, 6061.

19 J. Sato, N. Saito, H. Nishiyama and Y. Inoue, *J. Photochem. Photobiol., A*, 2002, **148**, 85.

20 J. J. Wang, L. Grocholl and E. G. Gillan, *Nano Lett.*, 2002, **2**, 899.

21 J. G. Li, L. Gao, J. Sun, Q. H. Zhang, J. K. Guo and D. S. Yan, *J. Am. Chem. Soc.*, 2001, **84**, 3045.

22 A. W. Jackson, O. Shebanova, A. L. Hector and P. F. McMillan, *J. Solid State Chem.*, 2006, **179**, 1383.

23 Y. Lee, H. Terashima, Y. Shimodaira, K. Teramura, M. Hara, H. Kobayashi, K. Domen and M. Yashima, *J. Phys. Chem. C*, 2007, **111**, 1042.

24 N. Zhang, S. Ouyang, T. Kako and J. Ye, *Chem. Commun.*, 2012, **48**, 1269.

25 F. Tessier, P. Maillard, Y. Lee, C. Bleugat and K. Domen, *J. Phys. Chem. C*, 2009, **113**, 8526.

26 C. Giordano, C. Erpen, W. Yao, B. Milke and M. Antonietti, *Chem. Mater.*, 2009, **21**, 5136.

27 C. Giordano, A. Kraupner, S. C. Wimbush and M. Antonietti, *Small*, 2010, **6**, 1859.

28 Z. Schnepp, S. C. Wimbush, M. Antonietti and C. Giordano, *Chem. Mater.*, 2010, **22**, 5340.

29 Q. Gao, C. Giordano and M. Antonietti, *Small*, 2011, **7**, 3334.

30 C. Giordano, C. Erpen, W. Yao and M. Antonietti, *Nano Lett.*, 2008, **8**, 4659.

31 C. R. Maunaye, *C. R. Seances Acad. Sci., Ser. C*, 1970, **270**, 2052.

32 R. W. Cumberland, R. G. Blair, C. H. Wallace, T. K. Reynolds and R. B. Kaner, *J. Phys. Chem. B*, 2002, **105**, 11922.

33 A. J. Anderson, R. G. Blair, S. M. Hick and R. B. Kaner, *J. Mater. Chem.*, 2006, **16**, 1318.